A LUNAR MICRO ROVER PATH PLANNING BASED ON ENVIRONMENTAL CONSTRAINTS

Takuto Oikawa[1], Shruti Keeni[1], Toshiki Tanaka[2], Kazuya Yoshida[1]

[1]*Tohoku University, Aoba 6-6-01, Aramaki, Aoba-ku, Sendai, Japan, E-mail: {oikawa,yoshida}@astro.mech.tohoku.ac.jp, shruti@keenis.com*
[2]*ispace Technologies, Inc., Azabudai 3-1-6, Iikura katamachi Annex 601, Minato-ku, Tokyo, E-mail: t-tanaka@ispace-inc.com*

ABSTRACT

In this paper, we will present various path planning choices when the rover is traveling under environmental constraints on the lunar surface. Three different environmental factors are considered to compute the optimal path: the lunar altitude map, the lunar surface temperature, and the solar direction. The altitude map and the surface temperature profile are obtained using the Lunar Laser Orbiter Altimeter and the Diviner Lunar Radiometer Experiment data, where both are scientific payloads inside the Lunar Reconnaissance Orbiter. The three attributes are combined in the form of a cost function to compute the least weighted path applied by Dijkstras algorithm. The resulting path, based on terramechanical behavior, rovers thermal response, and power generation, is solved in a heuristic manner to determine the rover's survivability and feasibility in a lunar condition.

1 INTRODUCTION

In the context of space exploration, effective path planning is important for rovers to conduct scientific missions in vast lunar/planetary surfaces. These types of rovers are usually remotely operated from ground. We have designed a lunar rover under Team HAKUTO, codenamed SORATO (shown in Figure 1), to be lightweight, compact and meet the minimum requirement for the Google Lunar XPRIZE (GLXP) challenge [?]. To increase the success of the GLXP mission, the operators need to be aware of its region of interest before they can cognitively choose the right optimal path. Thus, the rovers projected path needs to be simulated to determine the safest route to avoid any potential hazard in a remote area.

A number of motion planning studies have been conducted for lunar/planetary exploration based on environmental considerations: terramechanics [?, ?] and energy generation by solar cells [?, ?, ?]. A combination of the two external elements are also studied to determine the effective path based
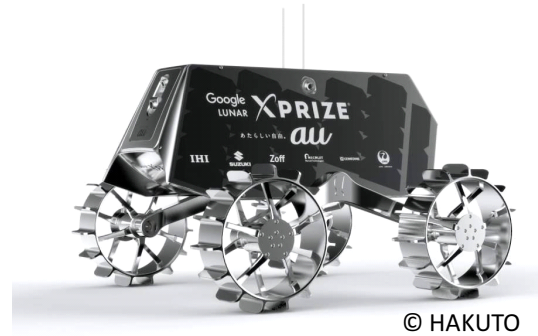

© HAKUTO

Figure 1: HAKUTO flight model rover

on the trade studies [?]. Using the solar incoming rays and lunar surface temperature conditions, thermally induced path planning is also studied [?].

This paper covers the following topics to evaluate the deterministic path. We start by defining the environmental conditions that the rover will experience during a potential mission. These constraints are incorporated into the prediction model of three rover attributes: traveling distance in a loose soil environment, thermal transient response, and power generation. We then compute a path planning simulation at specific lunar input condition.

2 LUNAR ENVIRONMENTS AND CONDITIONS

This section introduces the environmental constraints that are influential to the rover's path selection in the lunar conditions. These elements are determined during the pre-mission analysis by utilizing data from the payload on NASA's Lunar Reconnaissance Orbiter (LRO).

2.1 Digital Elevation Mapping

A global altitude map information is generated from the Lunar Laser Orbiter Altimeter (LOLA).[1]

---

[1]the LOLA data can be obtained from http://pds-geosciences.wustl.edu/missions/lro/lola.htm

This data creates elevation information at the corresponding latitude and longitude with a resolution of one-sixteenth of a degree. The height data from the LOLA is used to compute the local slopes at each available nodal point in latitude and longitude coordinates. This information decides whether the rover is capable of climbing or descending the nearing terrain. Any unfeasible region based on the slope map is denoted as an obstacle, and the threshold is chosen by experimental results from a controlled sandbed and terramechanical studies [**?**], shown in Section 3.1. The 3D map of the lunar surface based on the LOLA can also be visualized to determine approximate start and goal point for mission feasibility [**?**].

2.2 Surface temperature data

To determine the rover's survivability at several landing sites, surface temperature profiles at several latitudes are drawn in Figure 2, using the data from Diviner Lunar Radiometer Experiment (Diviner)[2] [**?**]. One lunar cycle temperature plots with different latitude are generated. We can observe that one lunar period is roughly 28 Earth days in duration, covering both lunar day and night at a continuous span of approximately two Earth weeks for each case. From the rover architecture, solar panels are the sole power source [**?**]. This limits the mission to span over a single lunar day as there are no other power sources inside the rover such as the radio-isotope thermal-electric generator to produce both power and heat during the night. Furthermore, the mission start time is another critical element to consider as the surroundings can be as cold as -200°C at sunrise. To avoid any failure from the extreme low temperature environment, we have defined that the mission should start at a minimum of 30 Earth hours after sunrise to reach the surface temperature at above -20°C. Depending on the target latitude, start-time will shift accordingly to accommodate the extreme temperature zone. For the lunar noon condition, the rover is designed to withstand the worst case thermal constraint in simulation [**?**].

Based on the Diviner data, Hurley et al. [**?**] successfully modeled the lunar surface temperature mathematically. For the lunar day condition, the temperature model (Eq 1) is represented in a function of solar zenith angle between the Moon-Sun line and the vector from the center of the Moon to the point on the lunar surface (ψ). The tuning
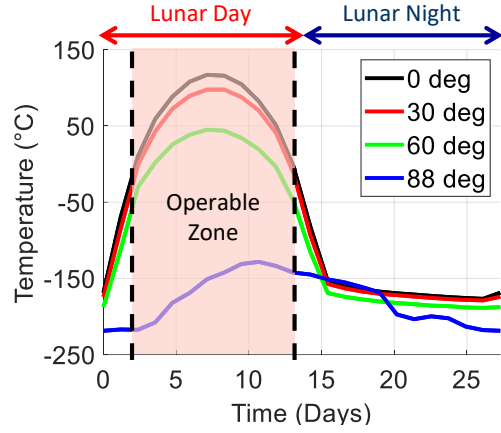
Figure 2: Lunar surface temperature profiles at different latitudes

factor of n is included to match the temperature profile in a sunlit condition. Furthermore, the one day lunar revolution at specific latitude (ϕ_{lat}) can be rearranged into earth-time (t) reference, where Oikawa et al. has defined it as following [**?**]:

$$T_l(\psi) = 392cos^n(\psi) > 130K \quad (\psi < 90°) \quad (1)$$

$$\psi(t) = \frac{2\pi}{T_p}\left|t - \frac{T_p}{4}\right|cos(\phi_{lat} + \phi_{inc}) \quad (2)$$

This equation is true if the temperature does not fall below a threshold of 130 K. Furthermore, ψ is rearranged into a time-variant function (t) to calculate the time of day in reference to the sun's position. Parameters such as the surface temperature at a target lunar latitude (ϕ_{lat}), overall lunar inclination angle (ϕ_{inc}), and lunar revolution period (T_p) are introduced to formulate the relationship. For the n power factor, we have changed the correction factor to 0.29 proposed by Walker [**?**] to reduce the daytime temperature model error to within 10°C when compared to the Diviner data instead of 0.25 by Hurley et al..

3 MATHEMATICAL MODELS

This section introduces the two different mathematical models to compute the lunar environmental conditions surrounding the rover.

3.1 Terramechanics model

When the rover is traveling in a lunar environment, we need to consider mobility performance over loose soil. One parameter that can quantify the rover's traversability in specific terrain conditions is the slip ratio, which is expressed as
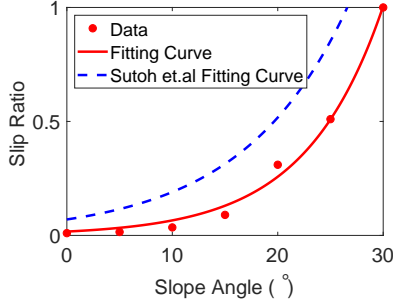
Figure 3: Rover's ascending performance in a sandy condition. The result is compared with Sutoh et al.'s wheeled rover's performance in a regolith simulant sandbox

$$s = \begin{cases} 1 - \frac{v_x}{r\omega}, & (|r\omega| \geq |v_x| : driving) \\ \frac{r\omega}{v_x} - 1, & (|r\omega| < |v_x| : braking) \end{cases} \quad (3)$$

, where v_x is the rover's velocity in the longitudinal direction, ω is the angular speed of the wheel, r is the wheel radius. By convention, the slip ratio is between -1 and 1. To quantify the amount of slippage on different slope angle, we conducted a slope ascending performance test using a sandbox testbed. Each run was tested in an increment of 5 degrees slope. The result is shown in Figure 3.

From the obtained data, a curve fit model in a function of slope angle on a longitudinal direction (θ_x) is generated with a confidence bound of 95%, shown in Eq 4.

$$s(\theta_y) = A \exp^{B\theta_y} \quad (4)$$

To show the validity of the exponential curve, we compared the slip ratio curve results from Sutoh et al. [?]. Although their wheels have been tested in a lunar regolith simulant, both rovers' performance has a similar tendency in the coefficient terms for Eq 4, shown in Table 1. To account for the actual mission scenario case under lunar regolith condition, we selected their results for the path planning simulation. For the simulation, we did not incorporate any side slip effect.

Table 1: Wheel parameters from experiment

Item	A	B
Wheel Result	0.01686	0.1363
Sutoh et al.'s Wheel Result	0.07	0.10

3.2 Thermal model

In this subsection, the thermal model is developed to evaluate the rover's thermal effect at a potential landing site.

3.2.1 Nomenclature

The symbols used in this section are defined below.

A_i : Surface area
A_w : Wheel-soil contact surface area
b : Surface albedo
$c_{p,i}$: Specific heat
$C_{i,j}$: Heat transfer coefficient
$F_{l,i}$: View factor from lunar surface to the rover
$F_{s,i}$: View factor from sun to the rover
m_i : Rover's mass
L_w : Wheel-soil contact length
P_s : Solar irradiance
$T_{r,i}$: Rover's temperature
T_{sp} : Outer space temperature
α_i : Solar absorptivity
ϵ_i : Rover's surface emissivity
ϵ_l : Lunar surface emissivity
λ : Thermal conductivity
σ : Stefan-Boltzmann constant

3.2.2 Heat transfer equation

Figure 4 shows the representative heat inputs and outputs from both the lunar environment and the inner body, where Q_s is the solar radiation from the sun, Q_a is the radiation from the surface albedo effect, Q_{lr} is the lunar surface radiation, Q_c is the conduction between the lunar surface and the rover, Q_e is the heat generated from on-board electronics, and Q_{sp} is the radiation emitted back to outer space. Assuming that each surface has a specific nodal point i, the following relation is derived to determine the general thermal equations.

$$Q_{in,i} = Q_{s,i} + Q_{a,i} + Q_{lr,i} + Q_c + Q_{e,i} - Q_{sp,i} \quad (5)$$

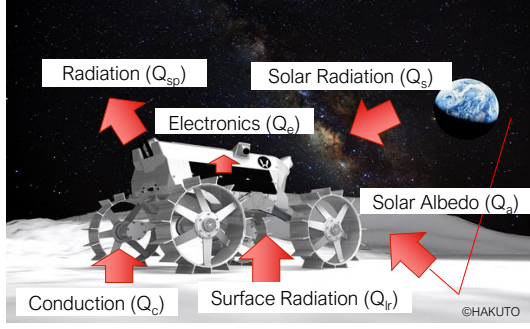Each heat transfer component is defined by the following equations.

Figure 4: External and internal heat input sources in lunar condition

$$Q_{s,i} = \alpha_i F_{s,i} A_i P_s \qquad (6)$$

$$Q_{a,i} = bQ_{s,i} \qquad (7)$$

$$Q_{lr,i} = \epsilon_i \epsilon_l F_{l,i} A_i \sigma(T_l^4 - T_{r,i}^4) \qquad (8)$$

$$Q_c = \lambda \frac{A_w}{L_w}(T_r - T_w) \qquad (9)$$

$$Q_e = constant \qquad (10)$$

$$Q_{sp,i} = \epsilon A F_{sp,i} \sigma(T_{r,i}^4 - T_{sp}^4) \qquad (11)$$

For the Q_e term, all on-board avionics are mounted only on the top, generating a direct heat source to the front, top, and rear surface area. This makes $Q_e = 0$ on the bottom section as none of the electronics are mounted on those surfaces. The electronics' mounting location is carefully selected to distribute the heat evenly per surface area while balancing the center of mass. This engineering decision was made to avoid the critical upper bound temperature during the lunar day-time [?]. Furthermore, the heat transfer effect from the Q_c term is negligible as the thermal conductivity between the lunar surface and the rover is low due to the wheel material selection. Therefore, we will omit this component from the equation.

To determine the transient response of the rover's surface temperature $T_{r,i}$, the following differential equation is established.

$$m_i c_{pi} \frac{dT_{r,i}}{dt} = Q_{in,i} - \sum_{j=1}^{6} C_{ij}(T_{r,i} - T_{r,j}) \qquad (12)$$
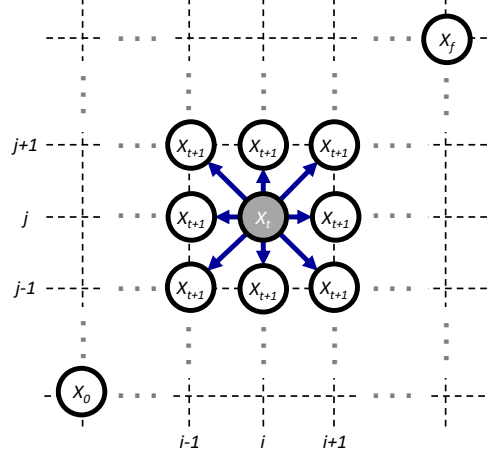

Figure 5: Definition of the grid, node, and edge for the algorithm

Note that we have another conduction parameter associated with surface nodes. With thermal-vacuum testing, we have determined that the thermal contact conductance $C_{i,j}$ between the rover's top section and the side panels, protected by a layer of low conductive polymide known as ULTEM, is $0.035\ W/K$. This value is inserted into the model to tune the response closer to the actual rover's characteristics. All necessary parameters to solve the ordinary differential equation can be found in Oikawa et al. [?].

4   PATH PLANNING SELECTION

This section introduces the path planning method based various environmental constraints. The underlying theories are described to incorporate the two different environmental constraints, and critical parameters are supplemented with experimental results.

4.1   Map Overview

Using the LOLA height map data with corresponding latitude and longitude information, we have implemented a grid-based map for the ease of computation, shown in Figure ??. We assume that the rover starts from an initial node of X_0 traveling incrementally to a target node of X_f along a path P. This path is generated in a time sequential manner from $\{X_0,...,X_f\}$. At time t, the rover's position is $X_t = (x_t, y_t, z_t)$, at a grid position (i, j). the rover can move in any of the eight directions on the map to node X_{t+1}. The distance d between the two nodes is defined as below:

$$d = \|X_{t+1} - X_t\| \qquad (13)$$

To devise the motion planning performance with the lunar environmental constraints, we have selected the Dijkstra's algorithm. By customizing each environmental element in the form of a cost function, the deterministic path for different case scenarios can be obtained by computing the minimum required cost. From each determined path P, we can obtain the total distance that the rover has traveled by summing the nodes that the rover travels inside the path P. A cost function for each environmental component is described in next section.

4.1.1 Algorithm and Cost Function

Considering that the rover is moving from node X_t to X_{t+1} with a neighborhood set of N_x. At node X_t, a cost function C_t exists. The motion between the two adjacent nodes outputs a unique cost function C_{t+1}, incorporating three environmental parameters and the distance traveled d.

$$C_{t+1} = C_t + d(W_{terra}C_{terra} + W_{th}C_{th} + W_pC_p) \tag{14}$$

C_{terra}, C_{th}, and C_p terms are the cost function associated to the terramechanics, thermal, and power generation respectively. Each of the elements is normalized to 1 in order to compare each cost function equally. The $\{W_{terra}$ W_{th}, and $W_p\}$ are the weighing factors for each environmental cost functions. They are set so that the summation of all three equals to 1. At Ct_f we can determine the total cost at the target goal. To determine the minimum path P based on the specific conditions, we take the $\text{argmin}(C_{t_f})$ to obtain the one "right route" among the other possible paths.

4.1.2 Terramechanics cost function

The rover's locomotive performance in loose soil conditions is expressed in a cost function using the predicted slip ratio s between the current node and the nearing node

$$C_{terra} = \frac{|s|}{s_{max}} \tag{15}$$

, where s_{max} is the maximum possible slip ratio that the rover can encounter during the simulation. For convenience, we assume that $s_{max} = 1$ when the rover's wheel starts to sink into the soil and thus immovable. The slip ratio between the nodes is computed using Eq 4 with the parameters from Table 1.

Algorithm 1 Djikstra's algorithm

Input: a weighted graph in a segmented grid map $\mathfrak{M} \in \mathbb{R}^2$ with a start point X_0, goal point X_f and constant environmental conditions
Result: $\text{Min}\{C(P) : P$ is a path determined by weighted environmental constraints$\}$
1: **while** $X_t \neq X_f$ **do**,
2:     compute neighborhood N_x with i direction (Euclidean distance)
3:     **for** $i \in N_x$ **do**
4:         Compute cost function c_i
5:     **end for**
6:     $C_{t+1} = C_t + c_i$
7:     Check $X_t = X_f$
8:     $t = t + 1$
9: **end while**
10: $\text{argmin}(X_{t+1})$
11: return path P

4.1.3 Thermal cost function

For the rover's temperature response, the thermal cost function is expressed in the following relation.

$$C_{th} = \begin{cases} \frac{1}{F_1}, & (T_{low,op} \leq T_r \leq T_{up,op}) \\ \frac{1}{F_2}, & (T_{low,tol} \leq T_r \leq T_{low,ol} \& T_{up,op} \leq T_r \leq T_{up,tol}) \\ 1, & otherwise \end{cases} \tag{16}$$

F_1 and F_2 are arbitrary factors defined based on rover's feasibility . This value does not hold any meaning other than to apply as a threshold value for the cost function.

Based on both operational and tolerable temperatures for each electronics, we have defined the threshold range for each surfaces on Table **??**.

Table 2: Feasible temperature range for avionics mounted surface with associated cost factor

Description		Requirement	Cost Factor
Front Surface	Operation Range	-40 ~ 85°C	50
	Tolerance Range	-40 ~ 100°C	5
Top Surface	Operation Range	0 ~ 40°C	50
	Tolerance Range	-5 ~ 45°C	5
Rear Surface	Operation Range	-40 ~ 85°C	50
	Tolerance Range	-40 ~ 100°C	5

4.1.4 Power generation cost

As part of the thermal model derivation, the rover's power generation from the solar ray's incoming direction to the rover is accounted for. A cost

function for power based path planning is shown below

$$C_p = 1 - \frac{P_{X_{t+1}}}{P_{max}} \qquad (17)$$

, where $P_{X_{t+1}}$ is the power generated at $t + 1$ and P_{max} is the maximum possible power generation available from the rover. To determine the maximum power during simulations, two case scenarios are considered

$$P_{max} = \begin{cases} \alpha \eta A P_s, & \text{if } F_s \leq 0.5 \\ 2\alpha \eta A F_s P_s, & \text{if } F_s > 0.5 \end{cases} \qquad (18)$$

, where η is the solar power efficiency, F_s is the view factor between solar radiation and the solar panel. When the $F_s \leq 0.5$, the maximum theoretical power generation is determined by computing the maximum power output of a single solar panel at F_s=1. Whereas in the case of $F_s > 0.5$, we assume that solar panel from both sides generates equal amount of power, which is beyond one sided solar panel generation.

5 PATH PLANNING RESULTS

5.1 Simulation Conditions

For the simulation environment, we have chosen the target site as Lacus Mortis (42.5-47.5°N,25-30°E) to explore the lunar skylight near Rimae Burg crater [?]. We assume that the rover starts from (46°N,25.5°E) and ends at (43.0625°N,28.5°E). Since the resolution of the lunar DEM from LOLA is not high, we have scaled the elevation model by 1000 times, creating the map of 150 m by 110 m. The simulation is computed in the worst case scenario, which is the lunar noon condition. This simulates the hottest case in this landing site. For the latitude information, we have chosen the average latitude in the grid, which is 45°N. The weighting factors in Eq ?? are set as {1,0,0}, {0,1,0}, and {0,0,1}, so that each attribute is assessed independently.

5.2 Simulation Result

The resulting path based on the terramechanical behavior (P_{terra}), thermal response(P_{th}), and power generation (P_p)is shown in Figure ??, and the profiles for each attribute are shown Figure ??. As we expect, P_{terra} is the shortest path among the three elements as it choses a route with minimal slip ratio. However, path P_{terra} failed to maintain
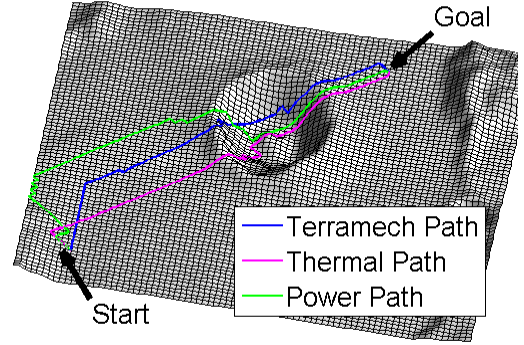

Figure 6: Path options for three different environmental constraints

the top surface temperature profiles within the operational range shown in Table ??. This suggests that the terramechanics component should not be the top priority weight factor for motion planning.

For both P_{th} and P_p, the temperature profile for all surfaces sustained above the operational temperature range threshold. The deciding difference between the two paths is the insolation condition as P_p avoided the shaded area as much as possible to generate power consistently. This increases the total traveling distance for path P_p by more than 30 meters than P_{th}.

6 CONCLUSION

In the mission planning stage for lunar exploration, environmental conditions are important factors to consider in order to predict the effective path based on the selected constraints. Depending on the path, different profiles are drawn, and each constraints have certain advantages over others, either in better locomotive performance, thermal control, or power generation. Further investigation is necessary in order to determine the "perfect" weight parameters to tune the parameters of choice based on the surrounding conditions. Furthermore, this simulation has only performed a single case scenario at specific latitude target. The algorithm's choice on deterministic path based on different latitude, mission analysis from the start and end duration with varying solar direction, and side slip effects will be studied in the future.

Acknowledgement

(a) Height to distance traveled

(b) Slip ratio to distance profile

(c) Power generation profile

(d) Top surface temperature profile

(e) Front surface temperature profile
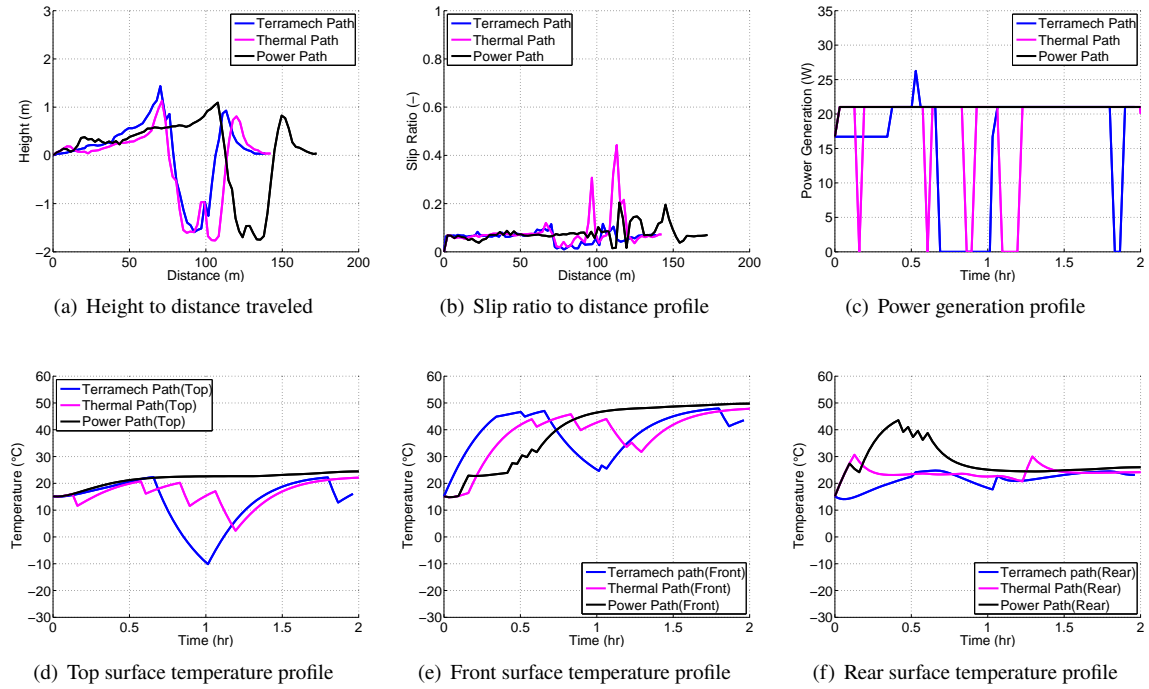
(f) Rear surface temperature profile

Figure 7: *Parameter outputs for three different environmental constraints*

References

[1] Walker J, Britton N, Yoshida K, Shimizu T, Burtz L and Pala A (2015) Qualification of Commercial Off-The-Shelf Components for a Lunar Rover Mission. In: *Proceedings of the 10th Conference on Field and Service Robotics*.

[2] Ishigami G, Nagatani K and Yoshida K (2011) Path Planning and Evaluation for Planetary Rovers Based on Dynamic Mobility Index. In: *2011 IEEE/RSJ International Conference on Intelligent Robots and Systems*. ISSN 2153-0858, pp.601–606. doi: 10.1109/IROS.2011.6094768.

[3] Trease B, Arvidson R, Lindermann R, Bennett K, Zhou F, Iagnemma K, Senatore C and Van Dyke L (2011) Dynamic Modeling and Soil Mechanics for Path Planning of the Mars Exploration Rovers. In: *International Design Engineering Technical Conferences and Computers and Information in Engineering Conference*. doi:doi: 10.1115/DETC2011-47896.

[4] Tompkins P, Stentz A and Whittaker W (2002) Mission planning for the Sun-Synchronous Navigation Field Experiment. In: *Proceedings 2002 IEEE International Conference on Robotics and Automation (Cat. No.02CH37292)*, volume 4, pp.3493–3500 vol.4. doi:10.1109/ROBOT.2002.1014251.

[5] Wettergreen D, Dias B, Shamah B, Teza J, Tompkins P, Urmson C, Wagner M and Whittaker W (2002) First experiment in sun-synchronous exploration. In: *Proceedings 2002 IEEE International Conference on Robotics and Automation (Cat. No.02CH37292)*, volume 4, pp.3501–3507 vol.4. doi:10.1109/ROBOT.2002.1014252.

[6] Otten ND, Wettergreen D and Whittaker W (2017) Strategic Autonomy for Reducing Risk of Sun-Synchronous Lunar Polar Exploration. In: *FSR*, volume 5 of *Springer Proceedings in Advanced Robotics*, Springer, pp.465–479.

[7] Sutoh M, Otsuki M, Wakabayashi S, Hoshino T and Hashimoto T (2015) The Right Path: Comprehensive Path Planning for Lunar Exploration Rovers. In: *IEEE Robotics Automation Magazine*, 22(1):pp.22–33. ISSN 1070-9932. doi: 10.1109/MRA.2014.2381359.

[8] Zuliani H, Oikawa T and Yoshida K (2017) Thermal Based Path Planning using Solar Orientaion for a Lunar Micro Rover. In: *Proceedings of the 31st International Space and Technology Symposium*, 2017-i-10.

[9] Bezdk A and Sebera J (2013) Matlab script for 3D visualizing geodata on a rotating globe. In: *Computers & Geosciences*, 56:pp.127 – 130. ISSN 0098-3004. doi:https://doi.org/10.1016/j.cageo.2013.03.007. URL `http://www.sciencedirect.com/science/article/pii/S000830041300068X`.

[10] Williams JP, Paige D, Greenhagen B and Sefton-Nash E (2017) The global surface temperatures of the Moon as measured by the Diviner Lunar Radiometer Experiment. In: *Icarus*, 283(Supplement C):pp.300–325. ISSN 0019-1035. doi:http://dx.doi.org/10.1016/j.icarus.2016.08.012.

[11] Oikawa T, Tanaka T, Walker J, Uno K, Costa P, Britton N and Yoshida K (2016) Thermal Design and Analysis of Conceptual Flight Model for a Lunar Exploration Rover. In: *Proceedings of the 13th International Symposium on Artificial Intelligence, Robotics and Automation in Space*.

[12] Hurley DM, Sarantos M, Grava C, Williams JP, Retherford KD, Siegler M, Greenhagen B and Paige D (2015) An analytic function of lunar surface temperature for exospheric modeling. In: *Icarus*, 255:pp.159 – 163. ISSN 0019-1035. doi:https://doi.org/10.1016/j.icarus.2014.08.043. URL `http://www.sciencedirect.com/science/article/pii/S0019103514004606`.

[13] Walker J (2016) *Scalable Flight System Design of Lunar Microrovers*. Doctoral Thesis, Tohoku University.

[14] Britton N, Yoshida K, Walker J, Nagatani K, Taylor G and Dauphin L (2013) Lunar Micro Rover Design for Exploration through Virtual Reality Tele-operation. In: *Field and Service Robotics*.